

From Heavy Rain Removal to Detail Restoration: A Faster and Better Network

Yuanbo Wen^a, Tao Gao^{a,*}, Jing Zhang^b, Kaihao Zhang^b, Ting Chen^a

^a*School of Information Engineering, Chang'an University, Xi'an 710064, China*

^b*School of Computing, Australian National University, Canberra, ACT 2600, Australia*

Abstract

The profound accumulation of precipitation during intense rainfall events can markedly degrade the quality of images, leading to the erosion of textural details. Despite the improvements observed in existing learning-based methods specialized for heavy rain removal, it is discerned that a significant proportion of these methods tend to overlook the precise reconstruction of the intricate details. In this work, we introduce a simple dual-stage progressive enhancement network, denoted as DPENet, aiming to achieve effective deraining while preserving the structural accuracy of rain-free images. This approach comprises two key modules, a rain streaks removal network (R²Net) focusing on accurate rain removal, and a details reconstruction network (DRNet) designed to recover the textural details of rain-free images. Firstly, we introduce a dilated dense residual block (DDRB) within R²Net, enabling the aggregation of high-level and low-level features. Secondly, an

*Corresponding author

Email address: tgaochd@126.com (Tao Gao)

¹The research was partially supported by the National Key R & D Program of China under Grants 2019YFE0108300 and the National Natural Science Foundation of China under Grants 52172379, 62001058 and U1864204.

enhanced residual pixel-wise attention block (ERPAB) is integrated into DR-Net to facilitate the incorporation of contextual information. To further enhance the fidelity of our approach, we employ a comprehensive loss function that accentuates both the marginal and regional accuracy of rain-free images. Extensive experiments conducted on publicly available benchmarks demonstrates the noteworthy efficiency and effectiveness of our proposed DPENet. The source code and pre-trained models are currently available at <https://github.com/chdwyb/DPENet>.

Keywords: Single image deraining, Detail reconstruction, Dual-stage network, Dilated convolution, Pixel-wise attention

1. Introduction

Images taken under inclement weather conditions experience a deterioration in their quality attributed to a multitude of factors [1, 2, 3]. Among these factors, the presence of rain streaks and the phenomenon known as the veiling effect [4, 5] induced by the scattering of light and the presence of water vapor, are particularly noteworthy. These degradations significantly exert a detrimental influence on the performance of computer vision algorithms [6, 7, 40]. Image deraining endeavors to eliminate rain streaks present in rainy images, thus addressing the degradation issue. Despite the substantial advancements made in deep deraining techniques [8, 9, 39, 10, 11, 12, 13, 14], we argue that the inherent complexities involving rain streaks, such as their density, size, and direction, as well as intricate compositional relationships between rain streaks and the background, continue to pose formidable challenges for the heavy rain removal.

Two primary challenges are evident in the context of heavy rain removal, namely the proficient representation of salient features pertaining to heavy rain [10, 15, 16], and the precise restoration of intricate details within rain-free images [9, 11, 8, 12, 17]. To encompass a broader contextual understanding for the purpose of rain representation, earlier investigations often resort to employing stride operations, resulting in rain-free images with diminished resolution. Subsequently, dilated convolution [18] emerges as an alternative approach to augmenting the receptive field while preserving image resolution.

To overcome the inherent limitations of the previously deraining methodologies, we introduce a dual-stage progressive enhancement network (DPENet) that primarily targets heavy rain removal. The development of DPENet is guided by key concepts in the field of computer vision, notably dilated convolution [18], dense connection [19], and pixel-wise attention mechanism. Specifically, the initial stage of our approach entails the construction of a rain streaks removal network (R^2 Net). The fundamental architectural component of R^2 Net is our specially crafted dilated dense residual block (DDR B). DDR B incorporates the principles of dense connection and incorporates dilated convolution techniques with varying dilated factors. These design decisions empower R^2 Net to attain a broader receptive field for precise feature extraction, concurrently facilitating the aggregation of multi-level features.

Furthermore, placing particular emphasis on the restoration of textural details, we develop an enhanced residual pixel-wise attention block (ERPAB). The ERPAB consists of a dual-pronged architecture, encompassing a parallel dilated fusion block (PDFB) and a pixel-wise attention block (PAB). PDFB utilizes parallel convolutions with diverse dilated factors, effectively capturing

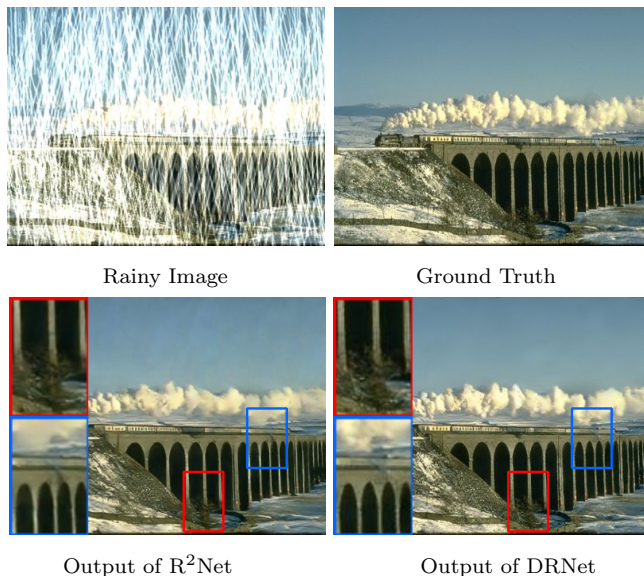


Figure 1: Our deraining results on a sample from Rain100H dataset [20]. Some Details of the coarsely derained image from R²Net are lost, while the details are richer after DRNet.

multi-field contextual information. Subsequently, PAB utilizes the output of the PDFB as its input, further enhancing the pixel-wise correlations and the spatial details. The core of our details reconstruction network (DRNet) lies the integration of ERPAB as a crucial constituent, thereby endowing DRNet with the capability to restore the structural intricacies of the initially coarsely derained images (as seen in Figure 1). Additionally, we introduce an innovative hybrid loss function designed to emphasize both marginal and regional accuracy aspects.

Figure 2 delineates the architectural panorama of our envisaged dual-stage progressive enhancement network. Our principal contributions may be succinctly encapsulated as follows.

- We introduce DPENet for the purpose of eliminating heavy rain degra-

dations. DPENet comprises two integral components, a dedicated rain streaks removal network and an intricately engineered details reconstruction network.

- Within R²Net, an intricate dilated dense residual block is introduced to proficiently acquire and discern salient attributes pertaining to precipitation, thereby facilitating the coarse restoration.
- Among DRNet, we introduce a refined residual pixel-wise attention block to facilitate the aggregation of image context and then reconstruct the textual details.
- Empirical findings on publicly available datasets substantiate both effectiveness and efficiency of our approach.

2. Related Work

Learning-based image deraining: Currently, learning-based image deraining establishes itself as the prevailing paradigm within the field [8, 9, 11, 21]. Following the seminal contribution of Fu *et al.*[8], which harnesses convolutional neural network (CNN) for the purpose of rain streaks elimination, a plethora of deep learning methodologies have been employed in image deraining, including residual learning [12, 22], recurrent architectures [9], models guided by prior knowledge [23, 14], generative networks [24], multi-scale pyramid approaches [10, 15], multi-stage learning strategies [25, 11, 21]. However, the synthetic datasets utilized for network training [20, 8] exhibit a notable lacuna in their failure to account for the veiling effect. Meanwhile,

a discernible limitation emerges within the domain of prevailing methodologies [9, 10, 15], wherein they largely neglect the details reconstruction in the context of rain streaks removal. This dual inadequacy inherent in extant techniques significantly curtails their efficiency when confronting with the exigencies of heavy rain scenarios.

Heavy rain removal: As delineated in [26], precipitation, specifically rain, induces image degradation through a dual-pronged mechanism. 1) Rain streaks exert a direct obscuring influence on the visual content of images. 2) Veiling effect, a secondary consequence of rain, further exacerbates the degradation. The extent of image quality deterioration stemming from light rain is generally constrained [27], while in stark contrast, heavy rain exhibits a profound capacity to inflict substantial damage upon image content [11], thereby presenting a formidable challenge in rain removal. Within the existing methodologies, [28] devises an approach that successfully detects and alleviates heavy rain within video sequences by virtue of an analysis centered on rain intensity. However, their method exhibits diminished efficiency when applied to static image devoid of temporal context. In [26], a comprehensive approach that encompasses both rain streaks and the veiling effect is adopted, which employs a synthesis of physical models and conditional generation learning techniques to effectuate the heavy rain removal. [29] employs a generative adversarial network (GAN) [30] to eliminate raindrops under conditions of heavy precipitation. Similarly, in alignment with the framework presented by [26], [31] utilizes a guided filter to segregate high-frequency and low-frequency components within the images degraded by heavy rain, thereby facilitating the extraction of rain streaks and atmo-

spheric light. Subsequently, they reconstruct rain-free images via a deep neural network. An overarching limitation observed across these methods is the isolated analysis and treatment of rain streaks and the veiling effect, thus overlooking potential inter-dependencies between the two degradations. This oversight culminates in the production of rain-free images that exhibit diminished structural fidelity [11]. Recently, with the application of multi-stage learning and multi-scale fusion, [15] and [21] achieve the superior performance in both light and heavy rain removal. However, these approaches do not explicitly account for the veiling effect during training and are further characterized by computationally intensive architectures, which consequently entails the protracted inference times.

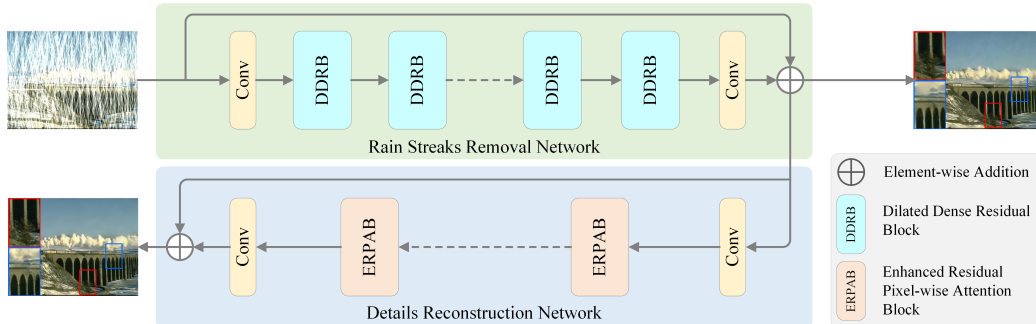


Figure 2: The architectural overview of the proposed dual-stage progressive enhancement network (DPENet), which consists of two sub-networks, namely a rain streaks removal network (R²Net) and a details reconstruction network (DRNet).

3. Proposed Method

In accordance with customary practice, our training dataset $D = \{x_i, y_i\}_{i=1}^N$ comprises multiple datasets [26, 20, 32, 8], where x_i and y_i denote the input rainy image and its corresponding ground truth, respectively. The index

i represents the individual images within the dataset, while N denotes the cardinality of the training dataset. In this work, we introduce a dual-stage progressive enhancement network designed for the purpose of proficient and effective heavy rain removal. The proposed network incorporates three key modules in its architecture, 1) a rain streaks removal network, responsible for eliminating rain artifacts from rainy images; 2) a details reconstruction network, dedicated to the restoration of fine-level details in the derained images; and 3) a hybrid loss function, which serves to emphasize the structural fidelity of the resulting rain-free images (refer to Figure 2). The primary objective of this endeavor is to establish a model for heavy rain removal with the aim of realizing the mapping $s = f_{\theta, \beta}(x)$ from a given rainy image x to its corresponding rain-free counterpart s . θ and β are the parameter sets associated with the rain streaks removal network and the details reconstruction network, respectively.

3.1. Rain Streaks Removal Network

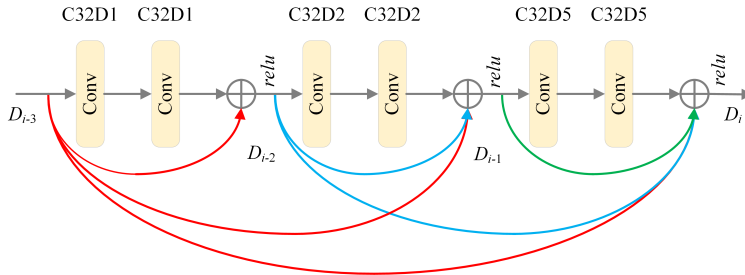


Figure 3: Illustration of our proposed dilated dense residual block (DDRB). C and D in (e.g. “C32D1”) denote the channel number and dilation rate of the dilated convolutional layer.

Rain streaks removal network accepts the rainy image x as its input and

yields a coarse derained image, represented as $s^c = f_\theta(x)$. Existing researches have demonstrated that residual learning [33] and densely-connected networks [19] exhibit the capability to capture inter-level feature correlations, thereby affording them a distinct advantage in achieving effective aggregation of high-level and low-level features. In this paper, we introduce the concept of dense residual block (DRB) to harness the advantages offered by both structural paradigms. The output R_i of i -th residual block (RB) is formulated as

$$\begin{aligned} R_i &= \sigma(W_2(\sigma(W_1 R_{i-1})) + R_{i-1}), i > 0, \\ R_i &= x, i = 0, \end{aligned} \tag{1}$$

where σ denotes the ReLU activation function, W_1 and W_2 are the weights of the 1st and 2nd convolutional layer, respectively. With dense connection, the output of DRB is

$$D_i = \sigma(W_i D_{i-1} + D_{i-1} + \dots + D_{i-n}), \tag{2}$$

where D_i is the i -th output in DRB, W_i is the weight of i -th residual block, n is the number of residual blocks before the i -th residual block. In this manner, the proposed DRB seamlessly incorporates all subsequent RB, thereby harnessing the advantages inherent in both residual learning and densely-connected networks. Our empirical investigations reveal that DRB exhibits superior efficiency in capturing features compared to a model solely relying on residual blocks.

In the context of rain removal, the concept of receptive field assumes particular significance. In order to further enhance the receptive field of DRB, we propose the incorporation of hybrid dilated convolution (HDC) [18] to

Table 1: Comparisons of the receptive filed modifications of DRB and DDRB.

DRB			
Convolution Layers	Kernel	Dilation	Receptive Field
1	3×3	1	3×3
2	3×3	1	5×5
3	3×3	1	7×7
4	3×3	1	9×9
5	3×3	1	11×11
6	3×3	1	13×13

DDRb			
Convolution Layers	Kernel	Dilation	Receptive Field
1	3×3	1	3×3
2	3×3	1	5×5
3	3×3	2	9×9
4	3×3	2	13×13
5	3×3	5	23×23
6	3×3	5	33×33

construct dilated dense residual block (DDRb) illustrated in Figure 3. Each instance of DDRb encompasses three RB and six ReLU nonlinear layers, with the additional incorporation of dense connections for the purpose of feature aggregation. Specifically, we establish dilation rates of [1, 1, 2, 2, 5, 5] to mitigate the gridding problem [18]. As illustrated in Table 1, through the utilization of dilated convolution, the receptive field expands from its initial dimensions of 13×13 to 33×33 , underscoring the efficiency of dilated convolution within the scope of our application, which is instrumental in achieving a more expansive receptive field. Subsequent to this, we incorporate several instances of DDRb and input/output (I/O) convolution layers to form the architecture of our R²Net. Moreover, a global skip connection is introduced to expedite training convergence. Our DDRb incorporates dense connections

to facilitate the aggregation of features from multiple levels, while employing dilated convolutions to extend the receptive field for the extraction of more precise features. These inherent advantages collectively empower our R²Net to effectively mitigate the presence of rain streaks at a coarse level, thereby resulting in an enhancement of overall performance.

3.2. Details Reconstruction Network

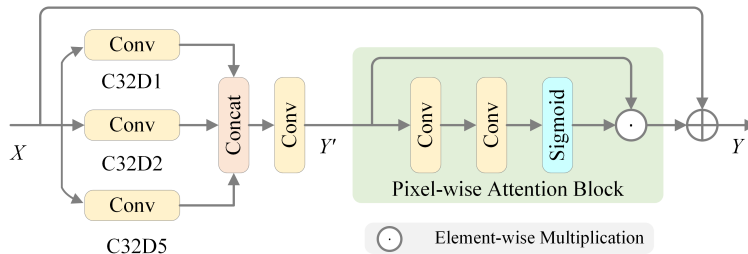


Figure 4: Illustration of our proposed enhanced residual pixel-wise attention block (ERPAB).

Existing deraining methods currently can be classified into two principal categories, namely the single-stage [8, 10, 34, 12] and multi-stage [9, 11, 21] networks. The former often yields rain-free images of sub-optimal quality. In tandem with the ongoing evolution of deraining researches, the multi-stage framework has progressively emerged as the prevailing paradigm. Nonetheless, these techniques have not been explicitly tailored to accommodate the inherent characteristics of images at distinct stages, thereby resulting in issues of image blurriness and misalignment in the final rain-free output, particularly under conditions of heavy rain. Consequently, in addition to the rain streaks removal network, we introduce a supplementary details reconstruction network designed to enhance the overall quality of the rain-free

images.

As depicted in Figure 4, DRNet takes the coarsely derained images as its input and the ultimate rain-free image can be formally defined as $s = f_{\theta,\beta}(x)$, wherein β signifies the parameters of DRNet. As elucidated in [11], it has been posited that the process of image deraining precipitates the inadvertent loss of textural details within the rain-free images. During the training regimen, a noteworthy strategy involves retraining the network by using degraded images in conjunction with ground truth as the target. This approach not only implicitly expands the training dataset but also facilitates the acquisition of a deeper understanding of the mapping relationship between coarsely derained images and their corresponding ground truth. Building upon the works in [20, 11, 21], we devise our details reconstruction network, which is founded on an enhanced pixel-wise residual attention block (ERPAB). This innovative block comprises a parallel dilated fusion block (PDFB) and a pixel-wise attention block (PAB). PDFB consists of three parallel dilated convolution layers for extracting context information and one convolution layer for fusing the features and aggregating contextual information.

PDFB is achieved via

$$Y' = \sigma(W_2(Cat \begin{pmatrix} W_{11,1}(X) \\ W_{12,2}(X) \\ W_{13,5}(X) \end{pmatrix}))), \quad (3)$$

where $W_{i,j,d}$ denotes the weight of dilated convolution of dilation rate d at i -th column and j -th, $Cat(\cdot)$ is concatenation operation, $X = s^c$ is the input of PDFB. PAB utilizes the output of PDFB as its input to further augment

the pixel-wise correlation, which can be formulated as

$$PAB(Y') = W_2(\sigma(W_1(Y'))) \cdot Y'. \quad (4)$$

Taking into consideration both PDFB and PAB, the proposed ERPAB is formulated as

$$s = \sigma(PAB(Y') + X). \quad (5)$$

Correspondingly, the variable $X = s^c$ represents the rain-free image at a coarse level. We employ multiple instances of ERPAB, input-output convolution layers, and a global skip connection scheme to establish our DRNet. The parameter setting of our proposed ERPAB is shown in Table 2. By amalgamating R²Net with DRNet, we successfully realize the proposed dual-stage progressive enhancement network. These networks collaboratively contribute to rain removal and the details reconstruction of the rain-free image $s = f_{\theta,\beta}(x)$.

Table 2: Parameters setting of our proposed ERPAB.

Convolution Layers	Kernel	Dilation	Input Channel	Output Channel
1.1	3×3	1	32	32
1.2	3×3	2	32	32
1.3	3×3	5	32	32
2	1×1	1	96	32
3	3×3	1	32	1
4	3×3	1	1	32

3.3. Hybrid Loss Function

The conventional mean square error (MSE), typically embraced within the domain of image deraining, exhibits commendable performance in the

assessment of peak signal-to-noise ratio (PSNR). Nevertheless, it is noteworthy that MSE frequently engenders outcomes characterized by excessive smoothing as a result of its quadratic penalization. Given the predominance of rain streaks within the high-frequency spectrum, it becomes opportune to employ the concept of edge loss [21] to quantify the fidelity of the rain-free image’s edges. This quantification may be formally expressed as

$$\mathcal{L}_{edge} = \frac{1}{H * W} \sum_{u=1}^H \sum_{v=1}^W \sqrt{|\Delta(s)_{u,v} - \Delta(y)_{u,v}|^2 + \varepsilon^2}, \quad (6)$$

where $\varepsilon = 10^{-3}$ is an offset value [21], $\Delta(\cdot)$ denotes the Laplacian operator.

As previously articulated, precipitation exhibits characteristics of marginality and regional specificity, and mitigating edge discrepancies can effectively address the challenge of edge accuracy. Additionally, the incorporation of structural similarity (SSIM) serves as a quantifiable metric for assessing the localized similarity between two images, denoted as (s and y). SSIM is defined as

$$SSIM(s, y) = \frac{2\mu_s\mu_y + C_1}{\mu_s^2\mu_y^2 + C_1} \cdot \frac{2\sigma_{sy} + C_2}{\sigma_s^2\sigma_y^2 + C_2}, \quad (7)$$

where μ_s and μ_y are the mean pixel value of the recovered rain-free image s and the corresponding ground truth y , respectively. σ_{sy} is the co-variance of s and y . σ_s, σ_y are the standard deviations of s and y . C_1, C_2 are constants. We have $C_1 = (K_1 * L)^2$, $C_2 = (K_2 * L)^2$, and generally $K_1 = 0.01$, $K_2 = 0.03$, $L = 255$ or 1 . We transmute the objective of maximizing SSIM into the pursuit of minimizing the ensuing mathematical construct, specifically denoted as the SSIM loss function

$$\mathcal{L}_{ssim} = 1 - SSIM(s, y). \quad (8)$$

By amalgamating the edge loss denoted as \mathcal{L}_{edge} with SSIM loss denoted as \mathcal{L}_{ssim} , we introduce a composite loss function

$$\mathcal{L}_{hybrid} = L_{ssim} + \gamma_e L_{edge}, \quad (9)$$

where γ_e is used to control the contribution of edge loss, and following [15] we set $\gamma_e = 0.05$.

4. Experiments

We present a comprehensive account of the experiments and the assessment outcomes encompassing synthetic as well as real-world rainy datasets. To elucidate the merits of our DPENet, we conduct a comparative analysis of its performance with ten cutting-edge methods, specifically DerainNet [8], SEMI [16], DIDMDN [23], UMRL [12], RESCAN [35], PReNet [9], JORDER-E [27], HRIR [26], MSPFN [15], and MPRNet [21].

4.1. Datasets

Our DPENet validation encompasses five synthetic datasets and one real-world dataset. Specifically, HeavyRain [26] and Rain100H [20] are comprised of images characterized by heavy rain, whereas Rain100L [20] constitutes the dataset featuring light rain conditions. Furthermore, the datasets Rain800 [32] and Rain1400 [8] encompass both heavy and light rain scenarios.

HeavyRain dataset is sourced from the released training dataset in [26]. The training dataset comprises a total of 9000 pairs of images. We partition this dataset into two distinct subsets, allocating 7500 pairs for training and reserving the remaining 1500 pairs for testing. Subsequently, we assign the nomenclature HeavyRain to this modified dataset configuration.

Rain100H dataset [20] is comprised of a collection of 1900 images randomly sourced from BSD [36]. The precipitation patterns within these images have been artfully generated through photo-realistic rendering methods or through the inclusion of simulated, distinct, and sharply defined linear streaks with different directions. In accordance with [20], this dataset encompasses a total of 1800 image pairs employed for training, encompassing five distinct streak orientations, while the evaluation phase utilizes 100 image pairs.

Rain100L dataset [20] comprises a curated selection of 300 high-quality images extracted from BSD [36]. Within this dataset, there are 200 image pairs specifically designated for training purposes, each characterized by a single category of rain streaks. Additionally, an additional set of 100 image pairs is allocated for the testing phase.

Rain800 dataset [32] is derived by employing a random selection procedure to identify 800 images randomly sourced from the UCID [37] and BSD [36] datasets. Subsequently, Zhang *et al.*[32] introduce rain streaks into these initially unaltered images through the use of Adobe Photoshop. Following this augmentation process, a subset comprising 700 image pairs is earmarked for training, while an additional subset of 100 image pairs is designated for testing.

Rain1400 dataset [8] employs a stochastic sampling approach to randomly select 1000 images from the UCID [37] dataset, BSD [36] dataset, and Google. Utilizing Adobe Photoshop, each pristine image undergoes a transformation process to yield 14 distinct rain-infused images characterized by varying rain streak orientations and magnitudes. The dataset encompasses a total of 12600 image pairs designated for training, alongside an additional 1400 image

pairs reserved for testing.

Real-world Rain dataset [10] comprises 300 authentic rainy images that encompass a diverse array of real-world environmental scenarios. This dataset serves to encapsulate a broad spectrum of scenes encountered in practical non-simulated settings.

4.2. Implementation Details

In R²Net, we employ a total of 10 DDRB, while in DRNet, 3 ERPAB are utilized. During the training phase, randomly cropped patches with size of 128×128 is executed, and the number of training epochs is set to 200. The batch size is configured to be 18, and the number of feature channels is established as 32. The optimization technique applied is the Adam optimizer, initialized with a learning rate of 1×10^{-3} , which undergoes a reduction of 0.2 at the 130th, 150th, and 180th epochs, respectively. All experiments are conducted on one NVIDIA Quadro RTX 4000 GPU.

4.3. Comparisons on Synthetic Rain Removal

As delineated in Section 2, images captured under heavy rain conditions exhibit the coexistence of densely distributed rain streaks and the atmospheric obscuration reminiscent of haze. To evaluate the efficiency of our proposed DPENet in mitigating the adverse effects of heavy rain coupled with haze, a series of experiments are conducted using HeavyRain dataset for comparisons of PReNet [9], HRIR [26], MPRNet [21] and our proposed DPENet. As illustrated in Table 3, DPENet manifests a noteworthy advantages in the context of heavy rain removal. More precisely, DPENet yields a substantial enhancement of 1.04 dB in PSNR and an augmentation of 2.26%

in SSIM compared to MPRNet [21]. This performance differential is further exemplified in Figure 5, where a visual comparison is presented, demonstrating that the proposed DPENet achieves preeminence in heavy rain removal. Notably, the derained images produced by DPENet exhibit finer details and a closer alignment with the ground truth.

Table 3: Quantitative results evaluated with respect to average PSNR and SSIM on HeavyRain dataset.

Metric	HRIR [26]	PReNet [9]	JORDER-E [27]	MPRNet [21]	DPENet
PSNR	21.73	24.01	24.79	25.13	26.17
SSIM	0.861	0.919	0.906	0.928	0.949

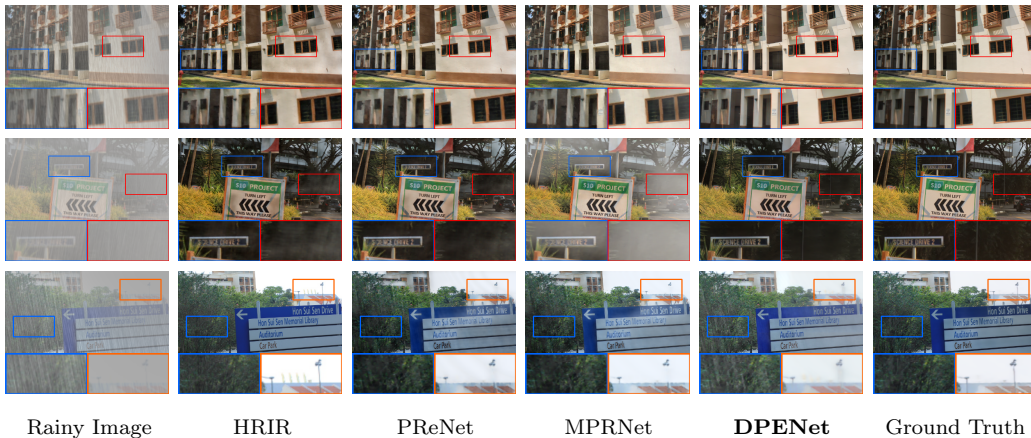


Figure 5: Image deraining results comparison with HRIR [26], PReNet [9], JORDER-E [27], MPRNet [21] and our DPENet on rainy images from HeavyRain dataset.

Additionally, we conduct a comparative analysis of our approach with eight other methodologies [8, 16, 23, 12, 35, 9, 27, 15] across four distinct publicly available datasets. The quantitative outcomes are presented in Table 4. As the results indicated, DPENet demonstrates a notable enhancement

in performance relative to the aforementioned eight methods. For instance, our DPENet outperforms DerainNet [8] and RESCAN [35] by 6.68 dB and 5.18 dB in terms of PSNR on Rain100H dataset [20]. Meanwhile, DPENet achieves superior performance on other datasets over other involved methods as well. Upon visual examination of the comparative results, as depicted in Figure 6, DPENet effectively eradicates rain streaks while simultaneously preserving intricate and trustworthy image details. Conversely, alternative methods tend to exhibit tendencies towards excessive smoothing or the retention of conspicuous rain streaks.

Table 4: Quantitative results evaluated with respect to average PSNR and SSIM on Rain100H [20], Rain100L [20], Rain800 [38] and Rain1400 [8] datasets.

Method	Rain100H		Rain100L		Rain800		Rain1400	
	PSNR	SSIM	PSNR	SSIM	PSNR	SSIM	PSNR	SSIM
DerainNet [8]	24.95	0.781	27.03	0.884	22.77	0.810	29.90	0.908
SEMI [16]	26.87	0.813	25.03	0.842	22.35	0.788	27.41	0.877
DIDMDN [23]	28.37	0.842	30.22	0.826	22.56	0.818	27.99	0.869
UMRL [12]	26.84	0.854	32.31	0.966	25.16	0.879	29.39	0.909
RESCAN [35]	26.45	0.846	35.67	0.967	24.09	0.841	32.03	0.931
PReNet [9]	29.46	0.899	37.48	0.979	26.61	0.902	32.55	0.946
JORDER-E [27]	24.54	0.802	37.10	0.980	27.08	0.872	32.39	0.940
MSPFN [15]	28.66	0.860	32.40	0.933	27.50	0.876	32.20	0.949
DPENet	31.63	0.924	39.20	0.984	27.82	0.903	32.77	0.951

4.4. Ablation Study

Components validation: DPENet comprises various fundamental constituents. In this section, we disassemble it into distinct constituent elements and substitute them with alternatives for conducting an ablation study. While adhering to the training strategy, we formulate five compar-

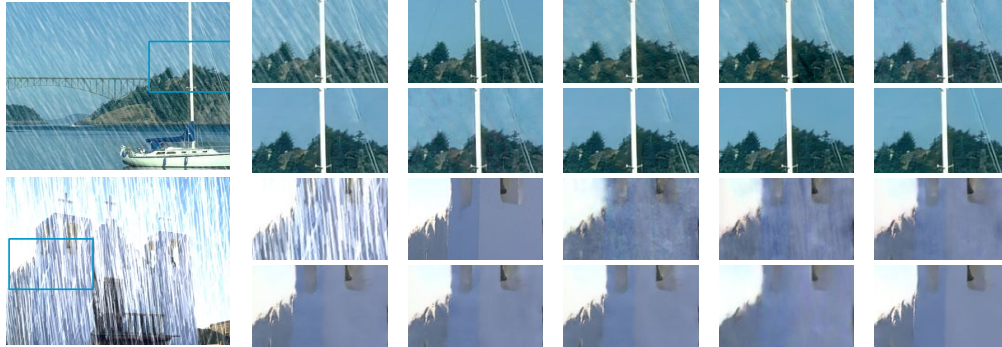


Figure 6: Visual comparisons of the evaluated methods. For single comparison, left is the rainy image. On the right, the first row from left to right that corresponds rainy patch, ground truth, and the results generated by DerainNet [8], SEMI [16], and DIDMDN [23], respectively. The second row from left to right corresponds the results produced by UMRL [12], RESCAN [35], PReNet [9], MSPFN [15], and our proposed DPENet.

ative models possessing an approximate equivalence in terms of parameter count to scrutinize the impact of our proposed DDRB and ERPAB systematically. The quantitative findings for the Rain100H dataset are enumerated in Table 5.

- **RB:** RB is the basic module to the whole network, which learns a function that maps the difference between input and output. It is easy to optimize and can improve performance by adding considerable depth.
- **DRB:** RB is replaced with dense residual block.
- **DDRB:** Introducing dilated convolution to DRB.
- **DDRB + PAB:** Our DPENet comprises R²Net based on the proposed DDRB and DRNet based on the proposed ERPAB. We use traditional

PAB for comparison.

- **DDR_B + ERPAB:** PAB is replaced by our proposed ERPAB, which is the proposed DPENet.

As delineated in Table 5, the PSNR exhibits an augmentation of 2.59 dB upon the incorporation of dilated convolutions and dense connections into the residual network. To substantiate the efficiency of ERPAB, we undertake a substitution of the PAB within the framework of DRNet. This substitution yields performance enhancements in contrast to preceding single-stage networks, with ERPAB manifesting an increment of 0.36 dB in PSNR. This also serves as corroboration for the structural efficiency of rain streaks removal network and detail reconstruction network. Furthermore, the comprehensive architecture comprising both DDR_B and ERPAB, surpasses alternative architectural configurations. We attribute this heightened performance to the inherent differentiation of deraining tasks at two distinct stages and the proficient representation of rain degradations within the proposed model.

Table 5: Quantitative comparisons of our DPENet with other network architectures on Rain100H dataset [20].

Methods	Without DRNet			With DRNet	
	RB	DRB	DDR _B	DDR _B +PAB	DPENet
PSNR	27.68	30.06	30.27	30.36	31.63
SSIM	0.876	0.904	0.907	0.909	0.924
Par.(M)	0.649	0.668	0.665	0.649	0.647

Parameter analysis on the number of DDR_B λ and ERPAB μ respectively: To assess the influence of variables denoted as λ and μ , we maintain one of these variables at a constant value while manipulating the

other to conduct controlled experiments. The outcomes obtained under various numerical configurations of DDRB and ERPAB are documented in Table 6. In scenarios where λ remains fixed, it is observed that the quality of rain-free images exhibits an improvement as μ is increased. This effect remains consistent when the roles of λ and μ are interchanged. Experimental findings reveal that in comparison to the configuration denoted as $\lambda_{10}\mu_3$, the configuration $\lambda_{15}\mu_3$ results in an augmentation of parameters by one-half, accompanied by a 0.04 dB increase in PSNR. Furthermore, the configuration $\lambda_{10}\mu_3$ yields a parameter increase of one-half as compared to $\lambda_5\mu_3$, with a corresponding 1.57 dB enhancement in PSNR. In order to strike a balance between effectiveness and efficiency, we set $\lambda = 10$ and $\mu = 3$ in our experimental investigations.

Table 6: Evaluation of the number of DDRB (λ) and ERPAB (μ) on Rain100H dataset [20] as well as the model parameters. $\lambda_a\mu_b$ denotes the network with $\lambda = a$ and $\mu = b$.

Methods	$\lambda_{15}\mu_3$	$\lambda_{15}\mu_1$	$\lambda_{10}\mu_3$	$\lambda_{10}\mu_1$	$\lambda_5\mu_3$	$\lambda_5\mu_1$
PSNR	31.67	31.60	31.63	31.35	30.06	28.91
SSIM	0.925	0.924	0.924	0.910	0.906	0.891
Par.(M)	0.924	0.861	0.647	0.585	0.371	0.308

Loss function analysis: Five distinct loss functions have been utilized to assess the performance of the light DPENet ($\lambda = 5$, $\mu = 3$) on Rain100H dataset [20]. The outcomes of this comparative analysis are presented in Table 7. In comparison to the employment of the L_{mse} loss function, the neural network trained with the \mathcal{L}_{edge} loss function exhibits a noteworthy enhancement of 3.2% in SSIM, while achieving comparable performance in PSNR. In light of these observations, we are prompted to explore an additional array of

hybrid loss functions denoted as $\mathcal{L}_{hybrid} = \mathcal{L}_{s+m}$, which is explicitly defined as

$$\mathcal{L}_{s+m} = \mathcal{L}_{ssim} + \gamma_{l2}\mathcal{L}_{mse}. \quad (10)$$

Following [15], we set $\gamma_{l2} = 1$. The performance of our model is presented in Table 7, wherein \mathcal{L}_{mse} , \mathcal{L}_{edge} , and \mathcal{L}_{ssim} denote models that have undergone training with individual loss functions, while \mathcal{L}_{s+m} signifies a model that has been trained utilizing the alternative hybrid loss function as specified in Equation 10. Furthermore, our hybrid loss function denoted as \mathcal{L}_{s+e} in Equation 9 has also been employed. Table 7 exhibits that both hybrid loss functions yield notably superior results in comparison to models trained solely with single loss functions. To be more precise, \mathcal{L}_{s+e} demonstrates an increase of 0.52 dB in PSNR when compared to \mathcal{L}_{s+m} , thereby elucidating the superior efficiency of the proposed hybrid loss function.

Table 7: Quantitative results of the light DPENet trained by five different loss functions on Rain100H dataset [20].

Loss Function	PSNR	SSIM
L_{mse}	28.96	0.8667
L_{edge}	28.88	0.8942
L_{ssim}	29.49	0.8986
L_{s+m}	29.54	0.8990
L_{s+e}	30.06	0.9063

Hyperparameter analysis: To verify the influence of different hyperparameters on the final rain removal performance of our proposed DPENet, we explore the effects of three hyperparameters, learning rate, batch size and patch size. As shown in the Table 8, when maintaining the same batch size and patch size, both high and low learning rate result in poor final rain re-

moval performance. In addition, since a smaller patch size will only result in worse performance than the current effect, we only discuss the case of a larger patch size. It should be noted that due to the limited computing resources, a larger patch size has to correspond to a smaller batch size. The results show that larger patch size does not bring better rain performance in our current experimental environment. Therefore, our training strategy enables our rain removal algorithm to achieve the best representation.

Table 8: Comparisons of training our proposed DPENet with different hyperparameters.

Training Strategy	Learning Rate	Batch Size	Patch Size	PSNR	SSIM
i	1×10^{-2}	18	128×128	23.71	0.785
ii	1×10^{-3}	18	128×128	31.63	0.924
iii	1×10^{-4}	18	128×128	28.44	0.883
iv	1×10^{-3}	6	224×224	29.18	0.901

4.5. Comparisons on Real-world Rain Removal

To assess the operational efficiency of DPENet within real-world scenarios and ascertain its capacity for generalization, we conduct supplementary experiments employing a real-world dataset derived from [10]. Analogously, we adopt two quantitative metrics, namely naturalness image quality evaluator (NIQE) and spatial-spectral entropy-based quality (SSEQ), to provide objective assessments of the performance concerning real-world rainy images. Table 9 presents a comprehensive overview of the quantitative outcomes, revealing that DPENet demonstrates superior performance when compared to other deraining techniques [12, 9, 15, 21]. Furthermore, Figure 7 showcases multiple deraining instances, offering visual comparisons. Notably, when inspecting the second rain-free image produced by alternative methodologies,

conspicuous rain streaks persist, accompanied by a degradation of fine details. In contrast, DPENet effectively mitigates the veiling phenomenon while simultaneously preserving textural details and mitigating the impact of rain streaks.

Table 9: QUantitative comparisons of average NIQE and SSEQ on the real-world dataset [10].

Methods	UMRL [12]	PReNet [9]	MSPFN [15]	MPRNet [21]	DPENet
NIQE	19.33	18.90	23.17	24.25	18.42
SSEQ	17.55	18.72	22.29	22.05	16.29

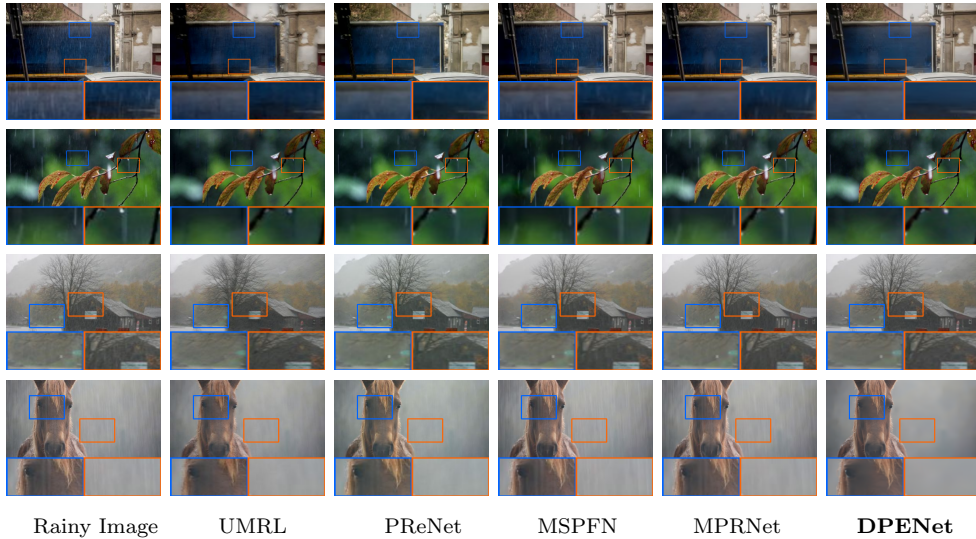


Figure 7: Visual comparisons of the derained results of UMRL [16], PReNet [9], MSPFN [15], MPRNet [21] and our DPENet on real-world rainy images [10].

4.6. Efficiency Analysis

To evaluate the efficiency of our proposed DPENet, we conduct a comparative analysis of four distinct methods, namely PReNet [9], JORDER-E

[27], MSPFN [15] and MPRNet [21]. The metrics utilized are average inference time (Ave. time), the quantity of trainable parameters (Par.) and the computational load measured in terms of floating-point operations (FLOPs) when processing 100 rainy images with size of 256×256 . The results of this examination are delineated in Table 10. Table 10 presents a conspicuous finding that DPENet registers the most favorable outcomes in average inference time and FLOPs. Specifically, it achieves a remarkable reduction of approximately 38.9% in inference time and a noteworthy decrease of approximately 36.1% in FLOPs when compared to PReNet [9]. Despite a relatively higher count of learnable parameters inherent in our method over PReNet, a careful comparison with JORDER-E, MSPFN, and MPRNet reveals that our approach exhibits superior efficiency and achieves the best trade-off between computational complexity and image quality.

Table 10: Efficiency analysis on 100 images with size of 256×256 .

Methods	PReNet [9]	JORDER-E [27]	MSPFN [15]	MPRNet [21]	DPENet
Ave. time (s)	0.036	0.098	0.249	0.058	0.022
Par. (M)	0.169	4.169	15.82	3.637	0.647
FLOPs (G)	66.44	272.7	605.3	141.5	42.43

4.7. Limitation Analysis

In addition to rain streaks and veiling effect, the authentic precipitation mapping may encompass deterioration factors, such as raindrops [41]. These factors are duly considered within our method and experimentation, thereby imposing constraints upon the practical applicability of our approach to a certain extent. Concurrently, our experimental procedures entail distinct train-

ing and testing conducted on separate datasets, resulting in a limited generalization capacity of our method across diverse datasets and complicated real-world scenarios. Furthermore, although our method is characterized by its lightweight and efficient nature, it does not exhibit discernible advantages in terms of the ultimate performance of rain removal when compared with other recent image deraining algorithms that necessitate substantial computational resources. Concerning the dual-stage loss function, our approach exclusively employs conventional loss functions to achieve the objectives of rain streaks elimination and fine-grained detail reconstruction. Regrettably, we omit the conceptualization and investigation of more purposive loss functions corresponding to different stages.

5. Conclusion

In this paper, we introduce DPENet, which is designed to attain a dual objective encompassing the proficient mitigation of heavy rain while adhering to stringent efficiency criteria. In contrast to antecedent methods that predominantly concentrate on the elimination of rain streaks, DPENet distinguishes itself by addressing the image deraining task as two stages, heavy rain mitigation and the restoration of textural details. This dual functionality is achieved through the deployment of a dedicated rain streaks removal network and a distinct network tasked with details reconstruction. Our investigation spans an extensive gamut of experiments conducted on six distinct datasets, encompassing both synthetically generated and real-world rain scenarios. These experiments serve to substantiate the efficiency of our proposed modules, namely DDRB and ERPAB. Furthermore, our findings underscore

the pivotal role played by multi-level feature fusion and the aggregation of contextual information in the domain of image deraining.

References

- [1] L. Wang, Y. Guo, Y. Wang, J. Li, S. Gu, R. Timofte, M. Cheng, H. Ma, Q. Ma, X. Sun, et al., Ntire 2023 challenge on stereo image super-resolution: Methods and results, in: Proceedings of the IEEE/CVF Conference on Computer Vision and Pattern Recognition, 2023, pp. 1346–1372.
- [2] T. Gao, Y. Wen, K. Zhang, J. Zhang, T. Chen, L. Liu, W. Luo, Frequency-oriented efficient transformer for all-in-one weather-degraded image restoration, *IEEE Transactions on Circuits and Systems for Video Technology* (2023).
- [3] Y. Li, Y. Zhang, R. Timofte, L. Van Gool, L. Yu, Y. Li, X. Li, T. Jiang, Q. Wu, M. Han, et al., Ntire 2023 challenge on efficient super-resolution: Methods and results, in: Proceedings of the IEEE/CVF Conference on Computer Vision and Pattern Recognition, 2023, pp. 1921–1959.
- [4] Z. Zhang, Y. Wei, H. Zhang, Y. Yang, S. Yan, M. Wang, Data-driven single image deraining: A comprehensive review and new perspectives, *Pattern Recognition* (2023) 109740.
- [5] K. Zhang, W. Luo, W. Ren, J. Wang, F. Zhao, L. Ma, H. Li, Beyond monocular deraining: Stereo image deraining via semantic understanding, in: *European Conference on Computer Vision*, Springer, 2020, pp. 71–89.

- [6] X. Chen, H. Li, M. Li, J. Pan, Learning a sparse transformer network for effective image deraining, in: Proceedings of the IEEE/CVF Conference on Computer Vision and Pattern Recognition, 2023, pp. 5896–5905.
- [7] Y. Wei, Z. Zhang, H. Zheng, R. Hong, Y. Yang, M. Wang, Sginet: Toward sufficient interaction between single image deraining and semantic segmentation, in: Proceedings of the 30th ACM International Conference on Multimedia, 2022, pp. 6202–6210.
- [8] X. Fu, J. Huang, X. Ding, Y. Liao, J. Paisley, Clearing the skies: A deep network architecture for single-image rain removal, *IEEE Transactions on Image Processing* 26 (6) (2017) 2944–2956.
- [9] D. Ren, W. Zuo, Q. Hu, P. Zhu, D. Meng, Progressive image deraining networks: A better and simpler baseline, in: *IEEE Conference on Computer Vision and Pattern Recognition*, 2019, pp. 3937–3946.
- [10] X. Fu, B. Liang, Y. Huang, X. Ding, J. Paisley, Lightweight pyramid networks for image deraining, *IEEE Transactions on Neural Networks and Learning Systems* 31 (6) (2019) 1794–1807.
- [11] S. Deng, M. Wei, J. Wang, Y. Feng, L. Liang, H. Xie, F. L. Wang, M. Wang, Detail-recovery image deraining via context aggregation networks, in: *IEEE Conference on Computer Vision and Pattern Recognition*, 2020, pp. 14560–14569.
- [12] R. Yasarla, V. M. Patel, Uncertainty guided multi-scale residual learning-using a cycle spinning cnn for single image de-raining, in: *IEEE*

- Conference on Computer Vision and Pattern Recognition, 2019, pp. 8405–8414.
- [13] K. Jiang, Z. Wang, C. Chen, Z. Wang, L. Cui, C.-W. Lin, Magic elf: Image deraining meets association learning and transformer, in: Proceedings of the 30th ACM International Conference on Multimedia, 2022, pp. 827–836.
- [14] W.-Y. Hsu, W.-C. Chang, Recurrent wavelet structure-preserving residual network for single image deraining, *Pattern Recognition* 137 (2023) 109294.
- [15] K. Jiang, Z. Wang, P. Yi, C. Chen, B. Huang, Y. Luo, J. Ma, J. Jiang, Multi-scale progressive fusion network for single image deraining, in: IEEE Conference on Computer Vision and Pattern Recognition, 2020, pp. 8346–8355.
- [16] W. Wei, D. Meng, Q. Zhao, Z. Xu, Y. Wu, Semi-supervised transfer learning for image rain removal, in: IEEE Conference on Computer Vision and Pattern Recognition, 2019, pp. 3877–3886.
- [17] K. Jiang, Z. Wang, P. Yi, C. Chen, Z. Wang, X. Wang, J. Jiang, C.-W. Lin, Rain-free and residue hand-in-hand: A progressive coupled network for real-time image deraining, *IEEE Transactions on Image Processing* 30 (2021) 7404–7418.
- [18] P. Wang, P. Chen, Y. Yuan, D. Liu, Z. Huang, X. Hou, G. Cottrell, Understanding convolution for semantic segmentation, in: IEEE Winter

- Conference on Applications of Computer Vision, IEEE, 2018, pp. 1451–1460.
- [19] G. Huang, Z. Liu, L. Van Der Maaten, K. Q. Weinberger, Densely connected convolutional networks, in: Proceedings of the IEEE conference on computer vision and pattern recognition, 2017, pp. 4700–4708.
- [20] W. Yang, R. T. Tan, J. Feng, J. Liu, Z. Guo, S. Yan, Deep joint rain detection and removal from a single image, in: IEEE Conference on Computer Vision and Pattern Recognition, 2017, pp. 1357–1366.
- [21] S. W. Zamir, A. Arora, S. Khan, M. Hayat, F. S. Khan, M.-H. Yang, L. Shao, Multi-stage progressive image restoration, in: IEEE Conference on Computer Vision and Pattern Recognition, 2021, pp. 14821–14831.
- [22] Y. Zhang, K. Zhang, Z. Chen, Y. Li, R. Timofte, J. Zhang, K. Zhang, R. Peng, Y. Ma, L. Jia, et al., Ntire 2023 challenge on image super-resolution (x4): Methods and results, in: Proceedings of the IEEE/CVF Conference on Computer Vision and Pattern Recognition, 2023, pp. 1864–1883.
- [23] H. Zhang, V. M. Patel, Density-aware single image de-raining using a multi-stream dense network, in: IEEE Conference on Computer Vision and Pattern Recognition, 2018, pp. 695–704.
- [24] Y. Wei, Z. Zhang, Y. Wang, M. Xu, Y. Yang, S. Yan, M. Wang, Deraincyclegan: Rain attentive cyclegan for single image deraining and rainmaking, *IEEE Transactions on Image Processing* 30 (2021) 4788–4801.

- [25] Y. Li, Y. Zhang, R. Timofte, L. Van Gool, Z. Tu, K. Du, H. Wang, H. Chen, W. Li, X. Wang, et al., Ntire 2023 challenge on image denoising: Methods and results, in: Proceedings of the IEEE/CVF Conference on Computer Vision and Pattern Recognition, 2023, pp. 1904–1920.
- [26] R. Li, L.-F. Cheong, R. T. Tan, Heavy rain image restoration: Integrating physics model and conditional adversarial learning, in: IEEE Conference on Computer Vision and Pattern Recognition, 2019, pp. 1633–1642.
- [27] W. Yang, R. T. Tan, J. Feng, Z. Guo, S. Yan, J. Liu, Joint rain detection and removal from a single image with contextualized deep networks, IEEE transactions on pattern analysis and machine intelligence 42 (6) (2019) 1377–1393.
- [28] C.-q. Ma, Z.-f. Liang, A rain detection and removal algorithm based on rainy intensity for videos in heavy rainy scene, in: International Conference on Oriental Thinking and Fuzzy Logic, Springer, 2016, pp. 657–667.
- [29] K. Matsumoto, F. Sakaue, J. Sato, Recovering raindrop removal images under heavy rain, in: VISIGRAPP (4: VISAPP), 2020, pp. 128–136.
- [30] I. Goodfellow, J. Pouget-Abadie, M. Mirza, et al. Generative adversarial nets, Advances in neural information processing systems, 2014, 27.
- [31] X. Pan, Y. Yang, C. Yang, C. Wang, A. Tan, Two-stage fusion model for heavy rain removal on single image, in: Journal of Physics: Conference Series, Vol. 2035, IOP Publishing, 2021, p. 012041.

- [32] H. Zhang, V. Sindagi, V. M. Patel, Image de-raining using a conditional generative adversarial network, *IEEE Transactions on Circuits and Systems for Video Technology* 30 (11) (2019) 3943–3956.
- [33] K. He, X. Zhang, S. Ren, J. Sun, Deep residual learning for image recognition, in: *IEEE Conference on Computer Vision and Pattern Recognition*, 2016, pp. 770–778.
- [34] Q. Guo, J. Sun, F. Juefei-Xu, L. Ma, X. Xie, W. Feng, Y. Liu, Efficient-derain: Learning pixel-wise dilation filtering for high-efficiency single-image deraining, *arXiv preprint arXiv:2009.09238* (2020).
- [35] X. Li, J. Wu, Z. Lin, H. Liu, H. Zha, Recurrent squeeze-and-excitation context aggregation net for single image deraining, in: *Proceedings of the European Conference on Computer Vision (ECCV)*, 2018, pp. 254–269.
- [36] P. Arbelaez, M. Maire, C. Fowlkes, J. Malik, Contour detection and hierarchical image segmentation, *IEEE transactions on pattern analysis and machine intelligence* 33 (5) (2010) 898–916.
- [37] G. Schaefer, M. Stich, Ucid: An uncompressed color image database, in: *Storage and retrieval methods and applications for multimedia 2004*, Vol. 5307, SPIE, 2003, pp. 472–480.
- [38] Y. Yang, H. Lu, Single image deraining via recurrent hierarchy enhancement network, in: *Proceedings of the 27th ACM International Conference on Multimedia*, 2019, pp. 1814–1822.

- [39] Y. Wen, T. Gao, Z. Li, J. Zhang, T. Chen, Multi-dimension queried and interacting network for stereo image deraining, arXiv preprint arXiv:2309.10319 (2023).
- [40] Y. Wen, T. Gao, J. Zhang, Z. Li, T. Chen, Encoder-free multi-axis physics-aware fusion network for remote sensing image dehazing, *IEEE Transactions on Geoscience and Remote Sensing* (2023).
- [41] Y. Wei, Z. Zhang, M. Xu, R. Hong, J. Fan, S. Yan, Robust attention deraining network for synchronous rain streaks and raindrops removal, in: *Proceedings of the 30th ACM International Conference on Multimedia*, 2022, pp. 6464–6472.